Electron- and neutrino-nucleus scattering in the impulse approximation regime

Omar Benhar[1,2], Nicola Farina[2], Hiroki Nakamura[3], Makoto Sakuda[4], and Ryoichi Seki[5,6]
[1] *INFN, Sezione di Roma. I-00185 Roma, Italy*
[2] *Dipartimento di Fisica, Università "La Sapienza". I-00185 Roma, Italy*
[3] *Department of Physics, Waseda University, Tokyo 160-8555, Japan*
[4] *Department of Physics, Okayama University, Okayama, 700-8530, Japan*
[5] *Department of Physics, California State University, Northridge, California 91330, USA*
[6] *W.K. Kellog Radiation Laboratory California Institute of Technology, Pasadena, California 91125, USA*

(Dated: February 2, 2008)

A quantitative understanding of the weak nuclear response is a prerequisite for the analyses of neutrino experiments such as K2K and MiniBOONE, which measure energy and angle of the muons produced in neutrino-nucleus interactions in the energy range $0.5 - 3$ GeV and reconstruct the incident neutrino energy to determine neutrino oscillations. In this paper we discuss theoretical calculations of electron- and neutrino-nucleus scattering, carried out within the impulse approximation scheme using realistic nuclear spectral functions. Comparison between electron scattering data and the calculated inclusive cross section off oxygen, at beam energies ranging between 700 and 1200 MeV, show that the Fermi gas model, widely used in the analysis of neutrino oscillation experiments, fails to provide a satisfactory description of the measured cross sections, and inclusion of nuclear dynamics is needed.

PACS numbers: 24.10.Cn,25.30.Fj,61.12.Bt

I. INTRODUCTION

The field of neutrino physics is rapidly developing after atmospheric neutrino oscillations and solar neutrino oscillations have been established [1, 2, 3]. Recently, the SK Collaboration has found evidence of the oscillatory signature in atmospheric neutrinos, improving the determination of Δm^2 [4], and K2K experiment has confirmed the oscillations of atmospheric neutrinos at 99.995% CL [5, 6]. These neutrino experiments measure energy and angle of muons produced in neutrino-nucleus interactions and reconstruct the incident neutrino energy, which determines the neutrino oscillations. K2K took data in the $E_\nu = 0.5 - 3$ GeV region, and the recent L/E analysis of the SK atmospheric neutrinos is mainly based on the dataset extending from 0.5 to 25 GeV. JPARC and NuMI neutrino experiments [7, 8] propose to measure $\nu_\mu \to \nu_e$ oscillations and determine Δm^2 with 1% accuracy and $\sin^2 2\theta_{13}$ above 0.006, using a narrow-band neutrino beam at $E_\nu = 0.8$ GeV (JPARC) and 2.0 GeV (NuMI, off-axis).

In view of these developments, it is vital that theoretical calculations of cross sections and spectra achieve an accuracy comparable to the experimental one, which in turn requires that the nuclear response to weak interactions be under control at a quantitative level.

At E_ν=3 GeV or less, quasi-elastic scattering and quasi-free Δ production are the dominant neutrino-nucleus processes. However, reactions in this energy regime are associated with a wide range of momentum transfer, thus involving different aspects of nuclear structure.

Four decades of electron-nucleus scattering experiments have unequivocally shown that the mean-field approximation, underlying the nuclear shell model, does not provide a fully quantitative account of the data (see, e.g., Ref. [9] and references therein). When the momentum transfer involved is large, dynamical nucleon-nucleon (NN) correlations are known to be important, and a description of nuclear structure beyond the mean-field picture is needed. On the other hand, neutrino-nucleus reactions also occur, in fact rather appreciably, with a small momentum transfer. Comparison between the data at $Q^2 < 0.2$ GeV^2 and the predictions of the Fermi gas (FG) model [10], showing a sizable deficit of events [6, 11], suggests that a more realistic description of both nuclear properties and the reaction mechanism is indeed required.

In this paper we discuss the extension of the many-body theory of electron-nucleus scattering (see, e.g., Ref. [12] and references therein) to the case of neutrino-induced reactions. We focus on the energy range $0.7-1.2$ GeV and analyze inclusive scattering of both electrons and neutrinos off oxygen, the main target nucleus in SK, K2K and other experiments. The quasi-elastic and quasi-free Δ production cross sections obtained from the FG model [10, 13] are compared to the results of the many-body approach developed in Ref. [14], extensively used

to analyze electron scattering data at beam energy up to few GeV [14, 15, 16]. Preliminary versions of the materials in this paper have appeared in the Proceedings of NuInt04 [9, 17, 18].

Section II is devoted to a summary of the formalism employed to calculate the electron-nucleus cross section at high momentum transfer, as well as to the discussion of the main ingredients entering its definition: the nuclear spectral function, the elementary cross section describing electron scattering off a *bound* nucleon and the folding function embodying the main effects of final state interactions.

In Section III the results of our approach are compared to inclusive electron scattering data at $0.2 \lesssim Q^2 \lesssim 0.6$ GeV^2, while in Section IV we outline the extension of the formalism to the case of charged current neutrino-nucleus scettering. Finally, our conclusions are stated in Section V.

II. MANY-BODY THEORY OF THE ELECTROWEAK NUCLEAR RESPONSE

A. Electron-nucleus cross section

The differential cross section of the process

$$e + A \to e' + X \ , \tag{1}$$

in which an electron carrying initial four-momentum $k \equiv (E_e, \mathbf{k})$ scatters off a nuclear target to a state of four-momentum $k' \equiv (E'_e, \mathbf{k}')$, the target final state being undetected, can be written in Born approximation as (see, e.g., Ref. [19])

$$\frac{d^2\sigma}{d\Omega_{e'} dE'_e} = \frac{\alpha^2}{Q^4} \frac{E'_e}{E_e} \, L_{\mu\nu} W^{\mu\nu} \ , \tag{2}$$

where α is the fine structure constant and $Q^2 = -q^2 = \mathbf{q}^2 - \nu^2$, $q = k - k' \equiv (\nu, \mathbf{q})$ being the four momentum transfer.

The leptonic tensor, that can be written, neglecting the lepton mass, as

$$L_{\mu\nu} = 2 \left[k_\mu k'_\nu + k_\nu k'_\mu - g_{\mu\nu}(kk') \right] \ , \tag{3}$$

is completely determined by electron kinematics, whereas the nuclear tensor $W^{\mu\nu}$ contains all the information on target structure. Its definition involves the initial and final hadronic states $|0\rangle$ and $|X\rangle$, carrying four-momenta p_0 and p_X, respectively, as well as the nuclear electromagnetic current operator J^μ:

$$W^{\mu\nu} = \sum_X \langle 0|J^\mu|X\rangle\langle X|J^\nu|0\rangle \delta^{(4)}(p_0 + q - p_X) \ , \tag{4}$$

where the sum includes all hadronic final states.

Calculations of $W^{\mu\nu}$ at moderate momentum transfers ($|\mathbf{q}| < 0.5$ GeV) can be carried out within nuclear many-body theory (NMBT), using nonrelativistic wave functions to describe the initial and final states and expanding the current operator in powers of $|\mathbf{q}|/m$, m being the nucleon mass (see, e.g., Ref. [20]). On the other hand, at higher values of $|\mathbf{q}|$, corresponding to beam energies larger than ~ 1 GeV, the description of the final states $|X\rangle$ in terms of nonrelativistic nucleons is no longer possible. Calculations of $W^{\mu\nu}$ in this regime require a set of simplifying assumptions, allowing one to take into account the relativistic motion of final state particles carrying momenta $\sim \mathbf{q}$ as well as the occurrence of inelastic processes, leading to the appearance of hadrons other than protons and neutrons.

B. The impulse approximation

The main assumptions underlying the impulse approximation (IA) scheme are that i) as the spatial resolution of a probe delivering momentum $\mathbf{q}$ is $\sim 1/|\mathbf{q}|$, at large enough $|\mathbf{q}|$ the target nucleus is seen by the probe as a collection of individual nucleons and ii) the particles produced at the interaction vertex and the recoiling (A − 1)-nucleon system evolve indipendently of one another, which amounts to neglecting *both* statistical correlations due to Pauli blocking and dynamical Final State Interactions (FSI), i.e. rescattering processes driven by strong interactions.

In the IA regime the scattering process off a nuclear target reduces to the incoherent sum of elementary processes involving only one nucleon, as schematically illustrated in Fig. 1.

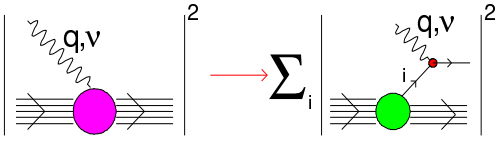

FIG. 1: (Color online) Pictorial representation of the IA scheme, in which the nuclear cross section is replaced by the incoherent sum of cross sections describing scattering off individual bound nucleons, the recoiling (A − 1)-nucleon system acting as a spectator.

Within this picture, the nuclear current can be written as a sum of one-body currents

$$J^\mu \to \sum_i j_i^\mu \ , \tag{5}$$

while the final state reduces to the direct product of the hadronic state produced at the electromagnetic vertex, carrying momentum $\mathbf{p}_x$ and the $(A-1)$-nucleon residual system, carrying momentum $\mathbf{p}_\mathcal{R} = \mathbf{q} - \mathbf{p}_x$ (for simplicity, we omit spin indices)

$$|X\rangle \to |x, \mathbf{p}_x\rangle \otimes |\mathcal{R}, \mathbf{p}_\mathcal{R}\rangle \ . \tag{6}$$

Using Eq. (6) we can rewrite the sum in Eq. (4) replacing

$$\sum_X |X\rangle\langle X| \;\rightarrow\; \sum_x \int d^3p_x |x,\mathbf{p}_x\rangle\langle \mathbf{p}_x,x| \times \sum_{\mathcal{R}} d^3p_{\mathcal{R}} |\mathcal{R},\mathbf{p}_{\mathcal{R}}\rangle\langle \mathbf{p}_{\mathcal{R}},\mathcal{R}| \; . \quad (7)$$

Substitution of Eqs. (5)-(7) into Eq. (4) and insertion of a complete set of free nucleon states, satisfying

$$\int d^3p \; |\mathrm{N},\mathbf{p}\rangle\langle \mathbf{p},\mathrm{N}| = I \; , \quad (8)$$

results in the factorization of the current matrix element

$$\langle 0|J^\mu|X\rangle \;=\; \frac{m}{\sqrt{\mathbf{p}^2_{\mathcal{R}}+m^2}} \langle 0|\mathcal{R},\mathbf{p}_{\mathcal{R}};\mathrm{N},-\mathbf{p}_{\mathcal{R}}\rangle \times \sum_i \langle -\mathbf{p}_{\mathcal{R}},N|j^\mu_i|x,\mathbf{p}_x\rangle \; , \quad (9)$$

leading to

$$W^{\mu\nu} \;=\; \sum_{x,\mathcal{R}} \int d^3p_{\mathcal{R}} \; d^3p_x |\langle 0|\mathcal{R},\mathbf{p}_{\mathcal{R}};\mathrm{N},-\mathbf{p}_{\mathcal{R}}\rangle|^2 \; \frac{m}{E_{\mathbf{p}_{\mathcal{R}}}} \times \sum_i \langle -\mathbf{p}_{\mathcal{R}},\mathrm{N}|j^\mu_i|x,\mathbf{p}_x\rangle\langle \mathbf{p}_x,x|j^\nu_i|\mathrm{N},-\mathbf{p}_{\mathcal{R}}\rangle \quad (10) \times \; \delta^{(3)}(\mathbf{q}-\mathbf{p}_{\mathcal{R}}-\mathbf{p}_x)\delta(\nu+E_0-E_{\mathcal{R}}-E_x),$$

where $E_{\mathbf{p}_{\mathcal{R}}} = \sqrt{|\mathbf{p}_{\mathcal{R}}|^2+m^2}$. Finally, using the identity

$$\delta(\nu+E_0-E_{\mathcal{R}}-E_x) \;=\; \int dE \delta(E-m+E_0-E_{\mathcal{R}}) \times \; \delta(\nu-E+m-E_x) \; , \quad (11)$$

and defining the target spectral function as [21]

$$P(\mathbf{p},E) \;=\; \sum_{\mathcal{R}} |\langle 0|\mathcal{R},-\mathbf{p};\mathrm{N},\mathbf{p}\rangle|^2 \times\delta(E-m+E_0-E_{\mathcal{R}}) \; , \quad (12)$$

we can rewrite Eq. (4) in the form

$$W^{\mu\nu}(\mathbf{q},\nu) \;=\; \sum_i \int d^3p \; dE \; w^{\mu\nu}_i(\widetilde{q}) \times \left(\frac{m}{E_{\mathbf{p}}}\right) P(\mathbf{p},E) \; , \quad (13)$$

with $E_{\mathbf{p}} = \sqrt{|\mathbf{p}^2|+m^2}$ and

$$w^{\mu\nu}_i \;=\; \sum_x \langle \mathbf{p},\mathrm{N}|j^\mu_i|x,\mathbf{p}+\mathbf{q}\rangle\langle \mathbf{p}+\mathbf{q},x|j^\nu_i|\mathrm{N},\mathbf{p}\rangle \times \; \delta(\widetilde{\nu}+\sqrt{\mathbf{p}^2+m^2}-E_x) \; . \quad (14)$$

The quantity defined in the above equation is the tensor describing electromagnetic interactions of the i-th nucleon *in free space*. Hence, Eq. (14) shows that in the IA scheme the effect of nuclear binding of the struck nucleon is accounted for by the replacement

$$q\equiv(\nu,\mathbf{q}) \rightarrow \widetilde{q}\equiv(\widetilde{\nu},\mathbf{q}) \; , \quad (15)$$

with (see Eqs. (10) and (12))

$$\begin{aligned}\widetilde{\nu} \;&=\; E_x - \sqrt{\mathbf{p}^2+m^2} \\ &=\; \nu + E_0 - E_{\mathcal{R}} - \sqrt{\mathbf{p}^2+m^2} \\ &=\; \nu - E + m - \sqrt{\mathbf{p}^2+m^2} \; , \end{aligned} \quad (16)$$

in the argument of $w^{\mu\nu}_i$. This procedure essentially amounts to assuming that: i) a fraction $\delta\nu$ of the energy transfer goes into excitation energy of the spectator system and ii) the elementary scattering process can be described as if it took place in free space with energy transfer $\widetilde{\nu} = \nu - \delta\nu$. This interpretation emerges most naturally in the $|\mathbf{p}| \ll m$ limit, in which Eq. (16) yields $\delta\nu = E$.

Collecting together all the above results we can finally rewrite the doubly differential nuclear cross section in the form

$$\frac{d\sigma_{IA}}{d\Omega_{e'}dE_{e'}} = \int \; d^3p \; dE \; P(\mathbf{p},E) \; \left[Z \frac{d\sigma_{ep}}{d\Omega_{e'}dE_{e'}} + (A-Z)\frac{d\sigma_{en}}{d\Omega_{e'}dE_{e'}} \right] \delta(\nu-E+m-E_x), \quad (17)$$

where $d\sigma_{eN}/d\Omega_{e'}dE_{e'}$ ($N\equiv n,p$ denotes a proton or a neutron) is the cross section describing the elementary scattering process

$$e(k) \; + \; N(p) \rightarrow e'(k') + x(p+\widetilde{q}) \; , \quad (18)$$

given by

$$\frac{d\sigma_{eN}}{d\Omega_{e'}dE_{e'}} = \frac{\alpha^2}{Q^4}\frac{E'_e}{E_e} \; \frac{m}{E_{\mathbf{p}}} L_{\mu\nu} w^{\mu\nu}_N \; , \quad (19)$$

stripped of both the flux factor and the energy conserving δ-function.

C. The nuclear spectral function

In NMBT the nucleus is seen as a system of A nucleons whose dynamics are described by the nonrelativistic hamiltonian

$$H_A = \sum_{i=1}^{A} \frac{\mathbf{p}_i^2}{2m} + \sum_{j>i=1}^{A} v_{ij} + \sum_{k>j>i=1}^{A} V_{ijk} \; , \quad (20)$$

where $\mathbf{p}_i$ is the momentum of the i-th nucleon, while v_{ij} and V_{ijk} are two- and three-nucleon interaction potentials, respectively.

The two-nucleon potential, that reduces to the Yukawa one-pion-exchange potential at large internucleon distance, is obtained from an accurate fit to the available

data on the two-nucleon system, i.e. deuteron properties and $\sim$ 4000 NN scattering phase shifts at energies up to the pion production threshold [22]. The additional three-body term V_{ijk} has to be included in order to account for the binding energies of the three-nucleon bound states [23].

The many-body Schrödinger equation associated with the Hamiltonian of Eq. (20) can be solved exactly, using stochastic methods, for nuclei with mass number $A \leq 10$. The energies of the ground and low-lying excited states are in excellent agreement with the experimental data [24]. Accurate calculations can also be carried out for uniform nucleon matter, exploiting translational invariace and using either a variational approach based on cluster expansion and chain summation techniques [25], or G-matrix perturbation theory [26].

Nonrelativistic NMBT provides a fully consistent computational framework that has been employed to obtain the spectral functions of the few-nucleon systems, having A= 3 [27, 28, 29] and 4 [15, 30, 31], as well as of nuclear matter, i.e. in the limit A $\rightarrow \infty$ with Z=A/2 [32, 33]. Calculations based on G-matrix perturbation theory have also been carried out for oxygen [34, 35].

The spectral functions of different nuclei, ranging from Carbon to Gold, have been modeled using the Local Density Approximation (LDA) [16], in which the experimental information obtained from nucleon knock-out measurements is combined with the results of theoretical calculations of the nuclear matter $P(\mathbf{p}, E)$ at different densities [16].

Nucleon removal from shell model states has been extensively studied by coincidence $(e, e'p)$ experiments (see, e.g., Ref. [36]). The corresponding measured spectral function is usually written in the factorized form

$$P_{MF}(\mathbf{p}, E) = \sum_n Z_n \ |\phi_n(\mathbf{p})|^2 F_n(E - E_n) \ , \qquad (21)$$

where $\phi_n(\mathbf{p})$ is the momentum-space wave function of the single particle shell mode state n, whose energy width is described by the function $F_n(E-E_n)$. The normalization of the n-th state is given by the so called spectroscopic factor $Z_n < 1$, and the sum in Eq. (21) is extended to all occupied states of the Fermi sea. Hence, $P_{MF}(\mathbf{p}, E)$ vanishes at $|\mathbf{p}|$ larger than the Fermi momentum $p_F \sim$ 250 MeV. Note that in absence of NN correlations $F_n(E-E_n)$ shrinks to a δ-function, $Z_n \equiv 1$ and Eq. (21) can be identified with the full spectral function.

Strong dynamical NN correlations give rise to virtual scattering processes leading to the excitation of the participating nucleons to states of energy larger than the Fermi energy, thus depleting the shell model states within the Fermi sea. As a consequence, the spectral function associated with nucleons belonging to correlated pairs extends to the region of $|\mathbf{p}| \gg p_F$ *and* $E \gg e_F$, where e_F denotes the Fermi energy, typically $\lesssim$ 30 MeV.

The correlation contribution to $P(\mathbf{p}, E)$ of uniform nuclear matter has been calculated by Benhar *et al* for a wide range of density values [16]. Within the LDA scheme, the results of Ref. [16] can be used to obtain the corresponding quantity for a finite nucleus of mass number A from

$$P_{corr}(\mathbf{p}, E) = \int d^3r \ \rho_A(\mathbf{r}) P^{NM}_{corr}(\mathbf{p}, E; \rho = \rho_A(\mathbf{r})) \ , \ (22)$$

where $\rho_A(\mathbf{r})$ is the nuclear density distribution and $P^{NM}_{corr}(\mathbf{p}, E; \rho)$ is the correlation component of the spectral function of uniform nuclear matter at density ρ.

Finally, the full LDA nuclear spectral function can be written

$$P_{LDA}(\mathbf{p}, E) = P_{MF}(\mathbf{p}, E) + P_{corr}(\mathbf{p}, E) \ , \qquad (23)$$

the spectroscopic factors Z_n of Eq. (21) being constrained by the normalization requirement

$$\int d^3p \ dE \ P_{LDA}(\mathbf{p}, E) = 1 \ . \qquad (24)$$

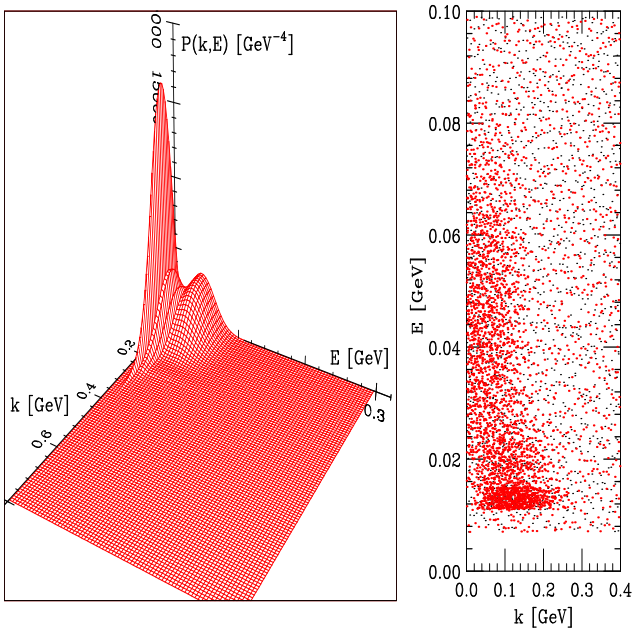

FIG. 2: (Color online) Three-dimensional plot (left panel) and scatter plot (right panel) of the oxygen spectral function obtained using the LDA approximation described in the text.

The LDA spectral function of ^{16}O obtained combining the nuclear matter results of Ref. [16] and the Saclay $(e, e'p)$ data [37] is shown in Fig. 2. The shell model contribution $P_{MF}(\mathbf{p}, E)$ accounts for $\sim$ 80 % of its normalization, whereas the remaining $\sim$ 20 % of the strength, accounted for by $P_{corr}(\mathbf{p}, E)$, is located at high momentum ($|\mathbf{p}| \gg p_F$) *and* large removal energy ($E \gg e_F$). It has to be emphasized that large E and large $\mathbf{p}$ are strongly correlated. For example, $\sim$ 50 % of the strength at $|\mathbf{p}| = 320$ MeV is located at $E > 80$ MeV.

The LDA scheme rests on the premise that short range nuclear dynamics is unaffected by surface and shell effects. The validity of this assumption is confirmed by

theoretical calculations of the nucleon momentum distribution, defined as

$$n(\mathbf{p}) = \int dE\ P(\mathbf{p},E) \quad (25)$$

$$= \langle 0|a^\dagger_{\mathbf{p}} a_{\mathbf{p}}|0\rangle\ , \quad (26)$$

where $a^\dagger_{\mathbf{p}}$ and $a_{\mathbf{p}}$ denote the creation and annihilation operators of a nucleon of momentum $\mathbf{p}$. The results clearly show that for A$\geq$ 4 the quantity $n(\mathbf{p})/A$ becomes nearly independent of A in the region of large $|\mathbf{p}|$ ($\gtrsim$ 300 MeV), where NN correlations dominate (see, e.g., Ref. [38]).

In Fig. 3 the nucleon momentum distribution of ^{16}O, obtained from Eq. (25) using the LDA spectral function of Fig. 2, is compared to the one resulting from a Monte Carlo calculation [40], carried out using the definition of Eq. (26) and a highly realistic many-body wave function [41]. For reference, the FG model momemtum distribution corresponding to Fermi momentum p_F = 221 MeV is also shown by the dashed line. It clearly appears that the $n(\mathbf{p})$ obtained from the spectral function is close to that of Ref.[40], while the FG distribution exhibits a completely different behaviour.

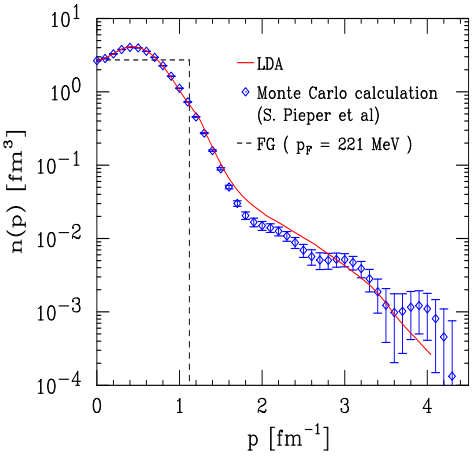

FIG. 3: (Color online) Momentum distribution of nucleons in the oxygen ground state. Solid line: LDA approximation. Dashed line: FG model with Fermi momentum p_F = 221 MeV. Diamonds: Monte Carlo calculation carried out by S.C. Pieper [40] using the wave function of Ref. [41].

A direct measuremet of the correlation component of the spectral function of ^{12}C, obtained measuring the $(e,e'p)$ cross section at missing momentum and energy up to $\sim$ 800 MeV and $\sim$ 200 MeV, respectively, has been recently carried out at Jefferson Lab by the E97-006 Collaboration [39]. The data resulting from the preliminary analysis appear to be consistent with the theoretical predictions based on LDA.

D. Final state interactions

The occurrence of strong FSI in electron nucleus scattering has long been experimentally established. The results of a number of $(e,e'p)$ measurements covering the kinematical domain corresponding to 0.5 $\lesssim Q^2 \lesssim$ 8.0 GeV^2 [42, 43, 44, 45], clearly show that the flux of outgoing protons is strongly suppressed, with respect to the IA predictions. The observed attenuation ranges from 20-40 % in Carbon to 50-70 % in Gold.

The inclusive (e,e') cross section, being only sensitive to rescattering processes taking place within a distance $\sim 1/|\mathbf{q}|$ of the electromagnetic vertex, is obviously much less sensitive to FSI than the coincidence $(e,e'p)$ cross section. The latter is in fact affected by rescatterings occurring over the distance $\sim R_A$, R_A being the nuclear radius, travelled by the struck particle on its way out of the target. However, FSI effects become appreciable, indeed dominant, in the low ν region, where the inclusive cross section is most sensitive to the high momentum and high removal energy tails of the nuclear spectral function.

In quasi-elastic inclusive processes FSI produce two effects: i) an energy shift of the cross section, due to the fact that the struck nucleon feels the mean field generated by the spectator particles and ii) a redistribution of the strength, leading to the quenching of the peak and the enhancement of the tails, to be ascribed to the occurrence of NN rescattering processes that couple the one particle-one hole final state to more complicated n particle-n holes configurations.

Early attempts to include FSI effects were based on the optical potential model [46]. However, while providing a computationally practical scheme to account for the loss of flux in the one-nucleon removal channel, this model relies on the mean field picture of the nucleus, and does not include the effect of dynamical NN correlations.

A different approach, based on NMBT and a generalization of Glauber theory of high energy proton scattering [47] has been proposed by Benhar et al. [14] in the early 90s. This treatment of FSI, generally referred to as Correlated Glauber Approximation (CGA) rests on the assumptions that i) the struck nucleon moves along a straight trajectory with constant velocity (eikonal approximation), and ii) the spectator nucleons are seen by the struck particle as a collection of fixed scattering centers (frozen approximation).

Under the above assumptions the expectation value of the propagator of the struck nucleon in the target ground state can be written in the factorized form

$$U_{\mathbf{p}+\mathbf{q}}(t) = U^0_{\mathbf{p}+\mathbf{q}}(t)\bar{U}^{FSI}_{\mathbf{p}+\mathbf{q}}(t)\ , \quad (27)$$

where $U^0_{\mathbf{p}+\mathbf{q}}$ is the free space propagator, while FSI effects are described by the quantity ($R \equiv (\mathbf{r}_1,\ldots,\mathbf{r}_A)$ specifies the target configuration)

$$\bar{U}^{FSI}_{\mathbf{p}+\mathbf{q}}(t) = \langle 0|U^{FSI}_{\mathbf{p}+\mathbf{q}}(R;t)|0\rangle\ , \quad (28)$$

with

$$U^{FSI}_{\mathbf{p}+\mathbf{q}}(R;t) = \frac{1}{A}\sum_{i=1}^{A} \mathrm{e}^{i\sum_{j\neq i}\int_0^t dt' w_{\mathbf{p}+\mathbf{q}}(|\mathbf{r}_{ij}+\mathbf{v}t'|)} \ . \quad (29)$$

In Eq. (29) $\mathbf{r}_{ij} = \mathbf{r}_i - \mathbf{r}_j$ and $w_{\mathbf{p}+\mathbf{q}}(|\mathbf{r}|)$ is the coordinate-space NN scattering t-matrix at incident momentum $\mathbf{p}+\mathbf{q}$, usually parametrized in terms of total cross section, slope and real to imaginary part ratio. At large $|\mathbf{q}|$, $\mathbf{p}+\mathbf{q} \approx \mathbf{q}$ and the eikonal propagator of Eq. (28) becomes a function of t and the momentum transfer only.

Note that $U^{FSI}_{\mathbf{q}}(R;t)$ is simply related to the nuclear transparency T_A, measured in coincidence $(e,e'p)$ experiments [42, 43, 44, 45], through

$$T_A = \lim_{t\to\infty} \langle 0||U^{FSI}_{\mathbf{q}}(R;t)|^2|0\rangle \ . \quad (30)$$

The results displayed in Fig. 4 [48] show that both the magnitude and the A- and Q^2-dependence of the transparencies of Carbon, Iron and Gold obtained from the approach of Ref. [14] and LDA are in good agreement with the experimental data. Note that at low Q^2 FSI lead to a $\sim$ 20 (40) % effect in Carbon (Iron). Neglecting this effect, i.e. setting $T_A(Q^2) \equiv 1$, would be utterly incompatible with the data.

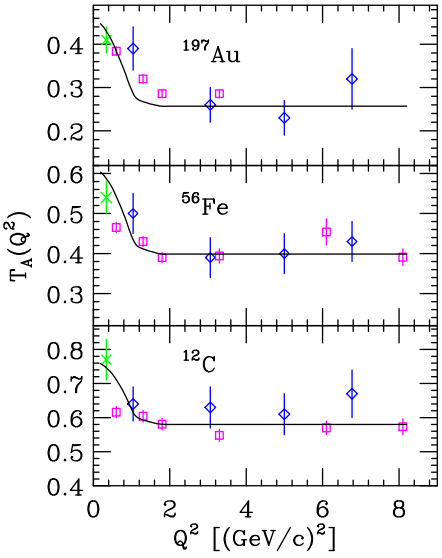

FIG. 4: (Color online) Q^2-dependence of the transparency of Carbon, Iron and Gold [48], calculated using LDA and the approach of ref.[14]. The data points are taken from Refs.[42] (crosses), [43] (diamonds) and [44, 45] (squares). Note that, in absence of FSI, $T_A(Q^2) \equiv 1$.

From Eqs. (28) and (29) it follows that within the approach of Ref. [14] the energy shift and the redistribution of the inclusive strength are driven by the real and the imaginary part of the NN scattering amplitude, respectively. At large $\mathbf{q}$ the imaginary part of $w_{\mathbf{q}}$, corresponding to the real part of $U^{FSI}_{\mathbf{q}}$, is dominant. Neglecting the contribution of the real part of $w_{\mathbf{q}}$ altogether, the CGA quasi-elastic inclusive cross section can be written as a convolution integral, involving the cross section evaluated within the IA, i.e. in absence of FSI, and a folding function embodying FSI effects:

$$\frac{d\sigma}{d\Omega_{e'}d\nu} = \int d\nu' \ f_{\mathbf{q}}(\nu-\nu') \ \left(\frac{d\sigma}{d\Omega_{e'}d\nu'}\right)_{IA} \ , \quad (31)$$

the folding function $f_{\mathbf{q}}(\nu)$ being defined as

$$f_{\mathbf{q}}(\nu) = \delta(\nu)\sqrt{T_A} + \int \frac{dt}{2\pi} \ \mathrm{e}^{i\nu t} \left[U^{FSI}_{\mathbf{q}}(t) - \sqrt{T_A}\right] \ . \quad (32)$$

The above equations clearly show that the strength of FSI is measured by both T_A and the width of the folding function. In absence of FSI $U^{FSI}_{\mathbf{q}}(R;t) \equiv 1$, implying in turn $T_A = 1$ and $f_{\mathbf{q}}(\nu) = \delta(\nu)$.

Dynamical NN correlations stronlgy affect the shape of the folding function of Eq. (32). Due to the strong repulsive core of the NN force, the joint probability of finding two nucleons at positions $\mathbf{r}_i$ and $\mathbf{r}_j$, driving the occurrence of rescattering processes in the final state, is strongly suppressed at $|\mathbf{r}_i - \mathbf{r}_j| \lesssim 1$ fm. As a consequence, inclusion of correlation effects within the framework of NMBT leads to a strong quenching of FSI effects, with respect to the predictions of the independent particle model.

In principle, the real part of the NN scattering ampliutde can be explicitely included in Eq. (29) and treated on the same footing as the imaginary part. However, its effect turns out to be appreciable only at $t \sim 0$, when the attenuation produced by the imaginary part is weak. The results of numerical calculations show that an approximate treatment based on the use of a time independent optical potential is indeed adequate to describe the energy shift produced by the real part of $w_{\mathbf{q}}$ [16], whose size of $\sim$ 10 MeV is to be compared to a typical electron energy loss of few hundreds MeV.

III. COMPARISON TO ELECTRON SCATTERING DATA

We have employed the formalism described in the previuos Sections to compute the inclusive electron scattering cross section off oxygen at $0.2 \lesssim Q^2 \lesssim 0.6$ GeV^2.

The IA cross section has been obtained using the LDA spectral function shown in Fig. 2 and the nucleon tensor defined by Eq. (14), that can be written as

$$w^{\mu\nu}_N = w^N_1 \left(-g^{\mu\nu} + \frac{\widetilde{q}^\mu \widetilde{q}^\nu}{\widetilde{q}^2}\right) + \frac{w^N_2}{m^2}\left(p^\mu - \frac{(p\widetilde{q})}{\widetilde{q}^2}q^\mu\right)\left(p^\nu - \frac{(p\widetilde{q})}{\widetilde{q}^2}q^\nu\right) \ , \quad (33)$$

where $p \equiv (E_{\mathbf{p}}, \mathbf{k})$ and the off-shell four momentum transfer $\widetilde{q}$ is defined by Eqs. (15) and (16). The two structure functions w^N_1 and w^N_2 are extracted from electron-proton and electron-deuteron scattering data.

In the case of quasi-elastic scattering they are simply related to the electric and magnetic nucleon form factors, G_{E_N} and G_{M_N}, through

$$w_1^N = -\frac{\widetilde{q}^2}{4m^2}\,\delta\left(\widetilde{\nu}+\frac{\widetilde{q}^2}{2m}\right)\,G_{M_N}^2\ , \qquad (34)$$

$$w_2^N = \frac{1}{1-\widetilde{q}^2/4m^2}\,\delta\left(\widetilde{\nu}+\frac{\widetilde{q}^2}{2m}\right) \times\left(G_{E_N}^2-\frac{\widetilde{q}^2}{4m^2}G_{M_N}^2\right)\ . \qquad (35)$$

Numerical calculations have been carried out using the Höhler-Brash parameterization of the form factors [49, 50], resulting from a fit which includes the recent Jefferson Lab data [51].

In the kinematical region under discussion, inelastic processes, mainly quasi-free Δ resonance production, are also known to play a role. To include these contributions in the calculation of the inclusive cross section, we have adopted the Bodek and Ritchie parametrization of the proton and neutron structure functions [52], covering both the resonance and deep inelastic region.

The folding functions describing the effect of NN rescattering in the final state have been computed from Eq. (32) with the eikonal propagator $U_{\mathbf{q}}^{FSI}(R;t)$ obtained using the parametrization of the NN scattering amplitude of Ref. [53] and the medium modified NN cross sections of Ref. [54]. The integrations involved in Eq. (28) have been carried out using Monte Carlo configurations sampled from the probability distribution associated with the oxygen ground state wave function of Ref. [41].

The effect of the real part of the NN scattering amplitude has been approximated including in the energy conserving δ-function of Eq. (17) the real part of the optical potential felt by a nucleon of momentum $\mathbf{p}+\mathbf{q}$ embedded in uniform nuclear matter at equilibrium density.

In Figs. 5-8 the results of our calculations are compared to the data of Ref. [55], corresponding to beam energies 700, 880, 1080 and 1200 MeV and electron scattering angle 32°. For reference, the results of the FG model corresponding to Fermi momentum $p_F = 225$ MeV and average removal energy $\epsilon = 25$ MeV are also shown.

Overall, the approach described in the previous Sections, *involving no adjustable parameters*, provides a fairly accurate account of the measured cross sections in the region of the quasi-free peak. On the other hand, the FG model, while yielding a reasonable description at beam energies 1080 and 1200 MeV, largely overestimates the data at lower energies. The discrepancy at the top of the quasi-elastic peak turns out to be ~ 25 % and ~ 50 % at 880 and 700 MeV, respectively.

The results of NMBT and FG model also turn out to be sizably different in the dip region, on the right hand side of the quasi-elastic peak, while the discrepancies become less pronounced at the Δ-production peak. However, it clearly appears that, independent of the employed approach and beam energy, theoretical results significantly underestimate the data at energy transfer larger than the pion production threshold.

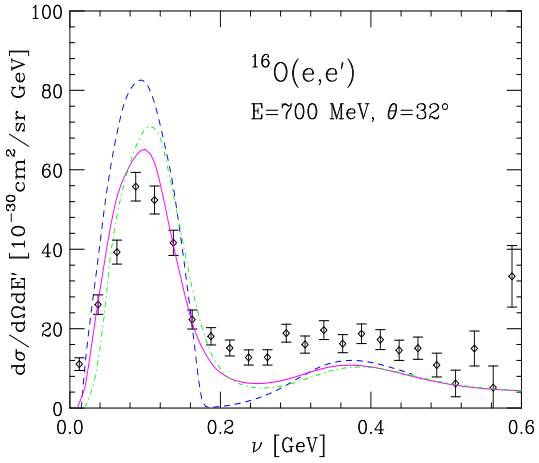

FIG. 5: (Color online) Cross section of the process $^{16}O(e,e')$ at beam energy 700 MeV and electron scattering angle 32°. Solid line: full calculation, carried out within the approach described in Section II. Dot-dash line: IA calculation, carried out neglecting FSI effects. Dashed line: FG model with $p_F = 225$ MeV and $\epsilon = 25$ MeV. The experimental data are from Ref.[55].

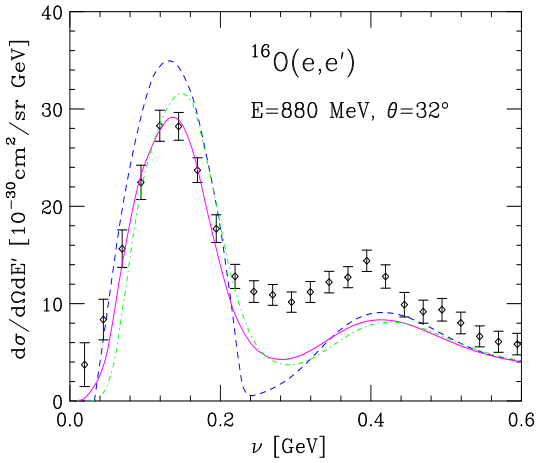

FIG. 6: (Color online) Same as in Fig. 5, but for beam energy 880 MeV.

In view of the fact that the quasi-elastic peak is correctly reproduced (within an accuracy of ~ 10 %), the failure of NMBT to reproduce the data at larger ω may be ascribed to deficiencies in the description of the elementary electron-nucleon cross section. In fact, as ilustrated in Fig. 9, the calculation of the IA cross section at the quasi-elastic and Δ production peak involves integrations of $P(\mathbf{p},E)$ extending over regions of the $(\mathbf{p},E)$ plane almost exaclty overlapping one another.

To gauge the uncertainty associated with the descrip-

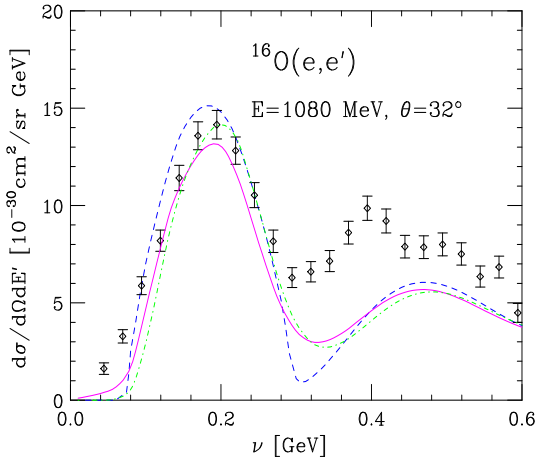

FIG. 7: (Color online) Same as in Fig. 5, but for beam energy 1080 MeV.

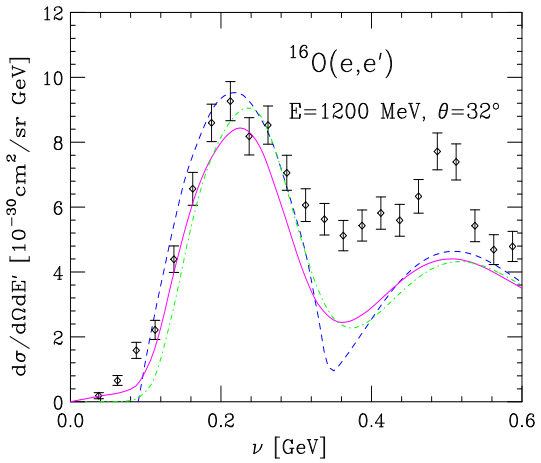

FIG. 8: (Color online) Same as in Fig. 5, but for beam energy 1200 MeV.

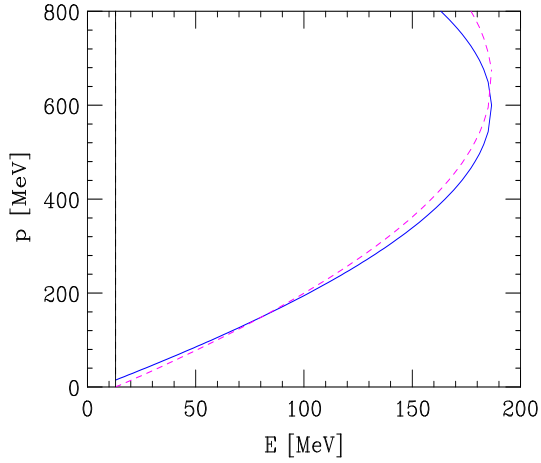

FIG. 9: (Color online) The solid and dashed lines enclose the integration regions in the $(\mathbf{p}, E)$ plane relevant to the calculation of the IA cross section at the top of the quasi-elastic and Δ production peak, respectively, for beam energy 1200 MeV and scattering angle 32°.

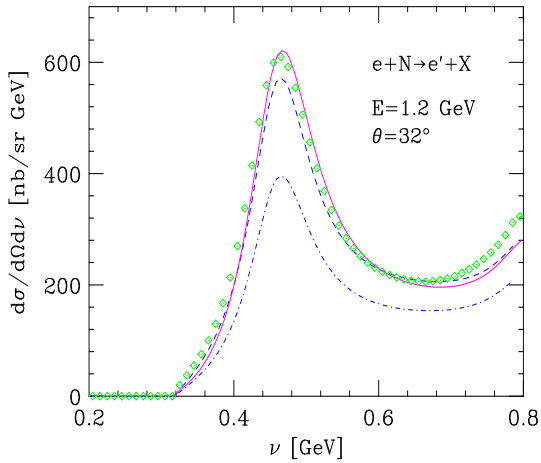

FIG. 10: (Color online) Cross section of the process $e + N \to e' + X$ above pion production threshold, at beam energy 1200 MeV and scattering angle 32°. Solid line: fit of Ref. [56] for ep scattering; dashed line: fit of Ref. [52] for ep scattering; diamonds: fit of Ref. [57] for ep scattering; dot-dash line: fit of Ref. [52] for en scattering.

tion of the nucleon structure functions w_1^N and w_2^N, we have compared the electron-proton cross sections obtained from the model of Ref. [52] to the ones obtained from the H_2 model of Ref. [56] and from a global fit including recent Jefferson Lab data [57]. The results of Fig. 10 show that at $E_e = 1200$ MeV and $\theta = 32°$ the discrepancy between the different models is not large, being ~ 15 % at the Δ production peak. It has to be noticed, however, that the models of Refs. [52, 56, 57] have all been obtained fitting data taken at electron beam energies larger than 2 GeV, so that their use in the kinematical regime discussed in this work involves a degree of extrapolation.

On the other hand, the results obtained using the approach described in this paper and the nucleon structure functions of Ref. [52] are in excellent agreement with the measured (e, e') cross sections at beam energies of few GeV [16]. As an example, in Fig. 11 we show a comparison between the calculated $^{12}C(e, e')$ cross section and the Jefferson Lab data of Ref. [58] at $E_e = 4$ GeV and $\theta = 30°$. The corresponding FG result is also displayed, for reference.

Fig. 10 also shows the prediction of the Bodek and Ritchie fit for the neutron cross section, which turns out to be much smaller than the proton one. It is on account of this difference that we have chosen to adopt the fit of Ref. [52], as it allows for a consistent inclusion of proton and neutron contributions, both resonant and nonresonsant, to the nuclear cross section. In this regard, it has to be pointed out that the nonresonant backround is not negligible. As illustrated in Fig. 12, for beam energy 1200 MeV and scattering angle 32° it provides ~ 25 % of the cross section at energy transfer corresponding to the

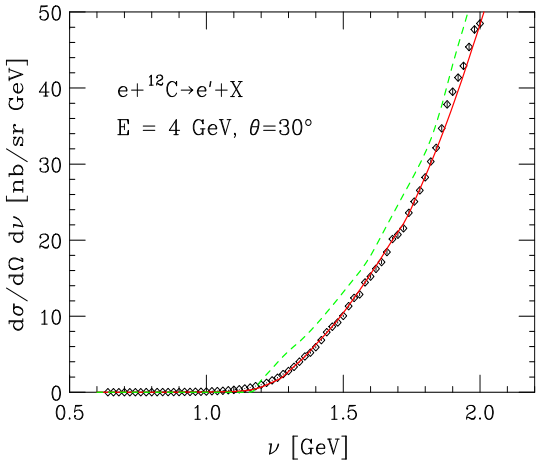

FIG. 11: (Color online) Cross section of the process $e+^{12}C \to e' + X$ at beam energy 4 GeV and scattering angle 32°. The solid line has been obtained using the approach described in this work, while the dashed line shows the results of the FG model corresponding to $p_F = 221$ MeV and $\epsilon = 25$ MeV. The experimental data are from Ref. [58].

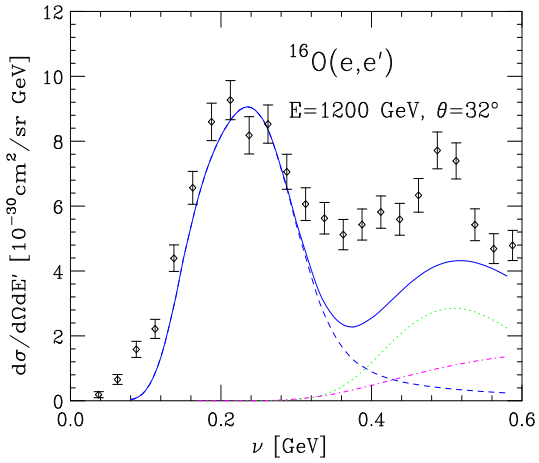

FIG. 12: (Color online) IA cross section of the process $^{16}O(e,e')$ at beam energy 1200 MeV and scattering angle 32°. Dashed line: quasi-elastic; dots: quasi-free Δ production; dashes: nonresonant background; solid line: total. The experimental data are from Ref. [55].

Δ peak.

The folding function described in Section II accounts for the FSI between a nucleon and the spectator system. For this reason, the results shown in Figs. 5-8 have been obtained folding with $f_{\mathbf{q}}(\nu)$ only the quasielastic component of the IA cross section. Particles other than protons and neutrons, that can be produced at the electromagnetic vertex, also have FSI, but they are more difficult to describe. However, the inelastic part of the IA cross section, being rather smooth, is unlikely to be strongly affected by FSI. To gauge the possible relevance of neglecting FSI in the inelastic channels we have computed the cross section at incident energy 880 MeV and scattering angle 32° folding the total IA result. Comparison with the results displayed in Fig. 6 shows a difference of ~ 0.5 % at the top of the Δ-production peak.

IV. CHARGED CURRENT NEUTRINO-NUCLEUS CROSS SECTION

The Born approximation cross section of the weak charged current process

$$\nu_\ell + A \to \ell^- + X \ , \tag{36}$$

can be written in the form (compare to Eq. (2))

$$\frac{d\sigma}{d\Omega_\ell dE_\ell} = \frac{G^2}{32\pi^2} \frac{|\mathbf{k}'|}{|\mathbf{k}|} L_{\mu\nu} W^{\mu\nu} \ , \tag{37}$$

where $G = G_F \cos\theta_C$, G_F and θ_C being Fermi's coupling constant and Cabibbo's angle, E_ℓ is the energy of the final state lepton and $\mathbf{k}$ and $\mathbf{k}'$ are the neutrino and charged lepton momenta, respectively. Compared to the corresponding quantities appearing in Eq. (2), the tensors $L_{\mu\nu}$ and $W^{\mu\nu}$ include additional terms resulting from the presence of axial-vector components in the leptonic and hadronic currents (see, e.g., Ref. [59]).

Within the IA scheme, the cross section of Eq. (37) can be cast in a form similar to that obtained for the case of electron-nucleus scattering (see Eq. (17)). Hence, its calculation requires the nuclear spectral function and the tensor describing the weak charged current interaction of a free nucleon, $w_N^{\mu\nu}$. In the case of quasi-elastic scattering, neglecting the contribution associated with the pseudoscalar form factor F_P, the latter can be written in terms of the nucleon Dirac and Pauli form factors F_1 and F_2, related to the measured electric and magnetic form factors G_E and G_M through

$$F_1 = \frac{1}{1 - q^2/4m^2} \left(G_E - \frac{q^2}{4m^2} G_M \right) \tag{38}$$

$$F_2 = \frac{1}{1 - q^2/4m^2} \left(G_M - G_E \right) \ , \tag{39}$$

and the axial form factor F_A.

Figure 13 shows the calculated cross section of the process $^{16}O(\nu_e, e)$, corresponding to neutrino energy $E_\nu = 1$ GeV and electron scattering angle $\theta_e = 30°$, plotted as a function of the energy transfer $\nu = E_\nu - E_e$. Numerical results have been obtained using the spectral function of Fig. 2 and the dipole parametrization for the form factors, with an axial mass of 1.03 GeV.

Comparison between the solid and dashed lines shows that the inclusion of FSI results in a sizable redistribution of the IA strength, leading to a quenching of the quasi-elastic peak and to the enhancement of the tails. For reference, we also show the cross section predicted by the FG model with Fermi momentum $p_F = 225$ MeV

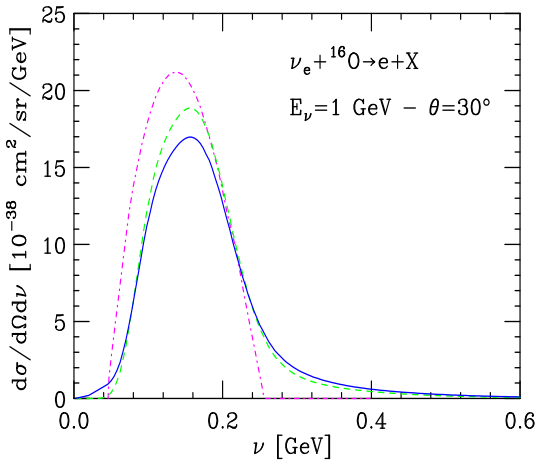

FIG. 13: (Color online) Differential cross section $d\sigma/d\Omega_e d\nu$ for neutrino energy $E_\nu = 1$ GeV and electron scattering angle $\theta_e = 30^\circ$. The IA results are represented by the dashed line, while the solid line corresponds to the full calculation, including the effects of FSI. The dotted line shows the prediction of the FG model with Fermi momentum $k_F = 225$ MeV and average separation energy $\epsilon = 25$ MeV.

and average separation energy $\epsilon = 25$ MeV. Nuclear dynamics, neglected in the oversimplified picture in terms of noninteracting nucleons, clearly appears to play a relevant role.

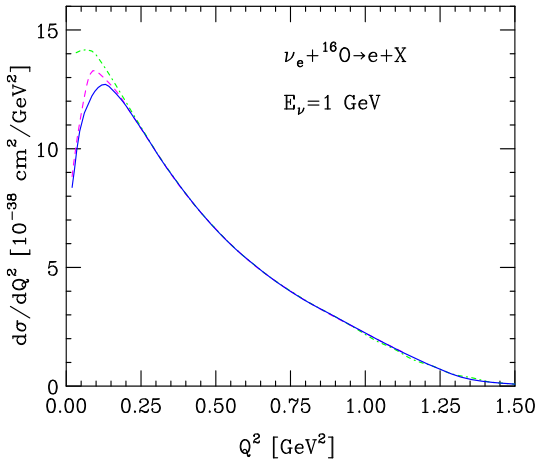

FIG. 14: (Color online) Differential cross section $d\sigma/dQ^2$ for neutrino energy $E = 1$ GeV. The dot-dash line shows the IA results, while the solid and dashed lines have been obtained using the modified spectral function ef Eq. (40), with and without inclusion of FSI, respectively. .

It has to be pointed out that the approach described in Section II, while including dynamical correlations in the final state, does not take into account statistical correlations, leading to Pauli blocking of the phase space available to the knocked-out nucleon.

A rather crude prescription to estimate the effect of Pauli blocking amounts to modifying the spectral function through the replacement

$$P(\mathbf{p}, E) \to P(\mathbf{p}, E)\theta(|\mathbf{p} + \mathbf{q}| - \overline{p}_F) \tag{40}$$

where $\overline{p}_F$ is the average nuclear Fermi momentum, defined as

$$\overline{p}_F = \int d^3r \; \rho_A(\mathbf{r}) p_F(\mathbf{r}), \tag{41}$$

with $p_F(\mathbf{r}) = (3\pi^2 \rho_A(\mathbf{r})/2)^{1/3}$, $\rho_A(\mathbf{r})$ being the nuclear density distribution. For oxygen, Eq. (41) yields $\overline{p}_F = 209$ MeV. Note that, unlike the spectral function, the quantity defined in Eq. (40) does not describe intrinsic properties of the target only, as it depends explicitely on the momentum transfer.

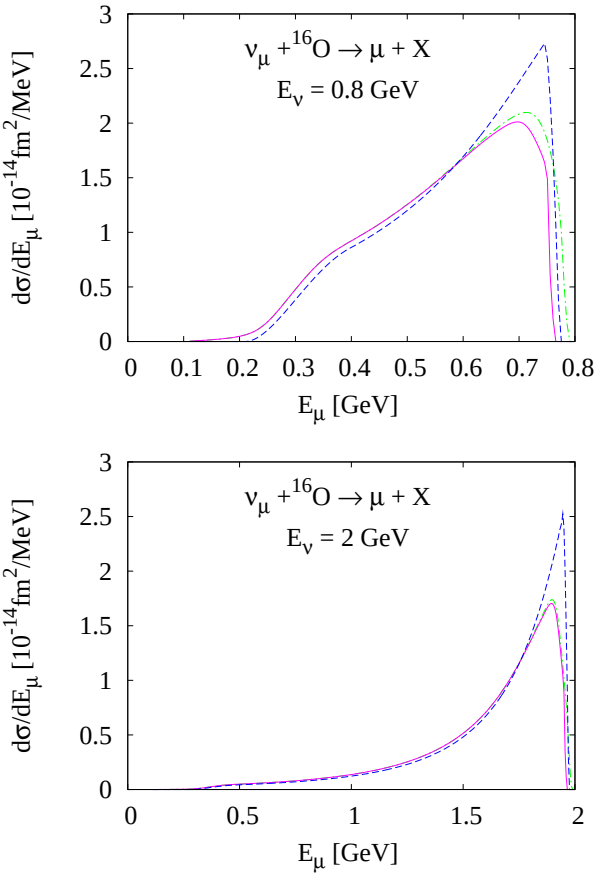

FIG. 15: (Color online) Quasi-elastic differential cross section $d\sigma/dE_\mu$ as a function of the scattered energy E_μ for the neutrino energy $E = 0.8$ and 2.0 GeV. The solid line shows IA calculation with Pauli blocking as in Eq. (40), the dot-dash line IA calculation without Pauli blocking, and the dashed line FG model.

The effect of Pauli blocking is hardly visible in the differential cross section shown in Fig. 13, as the kinematical setup corresponds to $Q^2 > 0.2$ GeV^2 at the quasi-elastic peak. The same is true for the electron scattering

cross sections discussed in the previous Section. On the other hand, this effect becomes very large at lower Q^2.

Figure 14 shows the calculated differential cross section $d\sigma/dQ^2$ for neutrino energy $E_\nu = 1$ GeV. The dashed and dot-dash lines correspond to the IA results with and without inclusion of Pauli blocking, respectively. It clearly appears that the effect of Fermi statistic in suppressing scattering shows up at $Q^2 < 0.2$ GeV^2 and becomes very large at lower Q^2. The results of the full calculation, in which dynamical FSI are also included, are displayed as a full line. The results of Fig. 14 suggest that Pauli blocking and FSI may explain the deficit of the measured cross section at low Q^2 with respect to the predictions of Monte Carlo simulations [11].

Figure 15 shows the ν_μ-nucleus cross sections as a function of the scattered muon energy, by comparing the cross sections calculated by FG, and by the use of the spectral function with and without Pauli blocking. Figure 15 shows that FG yields a larger high-energy peak contribution than the other two. This is *not* due to the Pauli blocking, but due to the nuclear correlation effects in the spectral function: the muons tend to be scattered with a higher energy. This effect should show up in the forward angle cross section and *may have a direct effect on neutrino oscillation measurements*.

V. CONCLUSIONS

We have employed an approach based on NMBT to compute the inclusive electron- and neutrino-nucleus scattering cross sections in the kinematical region corresponding to beam energy ~ 1 GeV, relevant to many neutrino oscillation experiments. Our calculations have been carried out within the IA scheme, using realistic spectral functions obtained from $(e, e'p)$ data and theoretical calculations of uniform nuclear matter.

In the region of the quasi-elastic peak, the results of our calculations account for the measured $^{16}O(e, e')$ cross sections at beam energies between 700 MeV and 1200 MeV and scattering angle 32° with an accuracy better than 10 %. It must be emphasized that the ability to yield quantitative predictions over a wide range of beam energies is critical to the analysis of neutrino experiments, in which the energy of the incident neutrino is not known, and must be reconstructed from the kinematics of the outgoing lepton.

In the region of quasi-free Δ production theoretical predictions significantly underestimate the data. Assuming the validity of the IA scheme, this problem appears to be mainly ascribable to uncertainties in the description of the nucleon structure functions in this kinematical regime. The upcoming electron-nucleus scattetring data in the resonance region from the Jefferson Lab E04-001 experiment [60] will help to shed light on this issue. At higher energies, i.e. in the region in which inelastic contributions largely dominate, the calculated cross sections are in close agreement with the data.

Among the mechanisms not included in the IA picture, scattering processes in which the incoming lepton couples to meson exchange currents are not expected to produce large corrections to our results in the region of the quasi-elastic peak. Numerical studies of the transverse response of uniform nuclear matter, carried out within NMBT [61], have shown that inclusion of two-body contributions to the nuclear electromagnetic current, arising from π and ρ meson exchange, leads to an enhancement that decreases as the momentum transfer increases, and never exceeds 10 % at $Q^2 < 0.25$ GeV^2. On the other hand, the results of calculations of the tranverse response of the few-nucleon systems (for a review see Ref. [20]) suggest that two-body current contributions may play a role in the dip region, at least for the lower values of the momentum transfer.

The second mechanism not included in the IA, Pauli blocking, while not appreciably affecting the lepton energy loss spectra, produces a large effect on the Q^2 distributions at $Q^2 < 0.2$ GeV^2, and must therefore be taken into account.

In conclusion, NMBT provides a fully consistent and computationally viable scheme to calculate the electroweak nuclear response. Using the approach discussed in this paper may greatly contribute to decrease the systematic uncertainties associated with the analysis of neutrino oscillation experiments, as, unlike the FG model and other many-body approaches based on effective NN interactions (see, e.g., Ref. [62] and references therein), it is strongly constrained by NN data and involves no adjustable parameters.

Acknowledgments

This work is supported by the U. S. Department of Energy under grant DE-FG03-87ER40347 at CSUN and by the U. S. National Science Foundation under grant 0244899 at Caltech. One of the authors (OB) is deeply indebted to Vijay Pandharipande and Ingo Sick for a number of illuminating discussions on issues relevant to the subject of this work. Thanks are also due to Steven Pieper for providing Monte Carlo configurations sampled from the oxygen ground state wave function of Ref. [41], as well as tables of the medium modified NN cross sections.

[1] Y. Fukuda *et al* (SK Collaboration), Phys. Rev. Lett. **81**, 1562 (1998).

[2] S. Fukuda *et al* (SK Collaboration), Phys. Lett. **B539**, 179 (2002);

Q.R. Ahmad *et al* (SNO Collaboration), Phys. Rev. Lett. **89**, 011301 (2002); **89**, 011302 (2002).
[3] K. Eguchi *et al* (KamLAND Collaboration), Phys. Rev. Lett. **90**, 021802 (2003).
[4] Y. Ashie *et al* (SK Collaboration), Phys. Rev. Lett. **93**, 101801 (2004).
[5] M.H. Ahn *et al* (K2K Collaboration), Phys. Rev. Lett. **90**, 041801 (2003).
[6] E. Aliu *et al* (K2K Collaboration), Phys. Rev. Lett. **94**, 081802 (2005).
[7] Y. Itow *et al*, hep-ex/0106019.
[8] M. Messier, talk at Neutrino 2004, Paris, June 2004.
[9] O. Benhar, Nucl. Phys. B (Proc. Suppl.) **139**, 15 (2005).
[10] R.A. Smith and E.J. Moniz, Nucl. Phys. **B43**, 605 (1972).
[11] T. Ishida, Nucl. Phys. B Proc. Suppl., **112**, 132 (2002).
[12] V.R. Pandharipande, Nucl. Phys. B (Proc. Suppl.), **112**, 51 (2002).
[13] H. Nakamura and R. Seki, Nucl. Phys. B (Proc. Suppl.) **112**, 197 (2002).
[14] O. Benhar *et al*, Phys. Rev. C **44**, 2328 (1991).
[15] O. Benhar and V.R. Pandharipande, Phys. Rev. C **47**, 2218 (1993).
[16] O. Benhar, A. Fabrocini, S. Fantoni and I. Sick, Nucl. Phys. **A579**, 493 (1994).
[17] H. Nakamura, R. Seki, and M. Sakuda, Nucl. Phys. B (Proc. Suppl.) **139**, 201 (2005).
[18] O. Benhar and N. Farina, Nucl. Phys. B (Proc. Suppl.) **139**, 230 (2005).
[19] C. Itzykson and J.B. Zuber, *Quantum Field Theory* (McGraw-Hill, New York, 1980).
[20] J. Carlson and R.Schiavilla, Rev. Mod. Phys. **70**, 743 (1998).
[21] As we will consider a target having N = Z = A/2, the spectral functions describing proton and neutron removal will be assumed to be the same.
[22] R.B. Wiringa, V.G.J. Stoks, R. Schiavilla, Phys. Rev. C **51**, 38 (1995).
[23] B.S. Pudliner, V.R. Pandharipande, J. Carlson, S.C. Pieper, R.B. Wiringa, Phys. Rev. C **56**, 1720 (1995).
[24] S.C. Pieper and R.B. Wiringa, Ann. Rev. Nucl. Part. Sci. **51**, 53 (2001).
[25] A. Akmal and V. R. Pandharipande, Phys. Rev. C **56**, 2261 (1997).
[26] M. Baldo, G. Giansiracusa, U. Lombardo, H.Q. Song, Phys. Lett. **B473**, 1 (2000).
[27] A.E.L. Dieperink, T. de Forest and I. Sick, Phys. Lett. **B63**, 261 (1976).
[28] C. Ciofi degli Atti, E. Pace and G. Salmè, Phys. Rev. C **21**, 805 (1980).
[29] H. Meier-Hajduk, Ch. Hadjuk and P.U. Sauer, Nucl. Phys. **A395**, 332 (1983).
[30] C. Ciofi degli Atti, S. Liuti and S. Simula, Phys. Rev. C **41**, R2474 (1990).
[31] H. Morita and T. Suzuki, Prog. Theor. Phys. **86**, 671 (1991).
[32] O. Benhar, A. Fabrocini and S. Fantoni, Nucl. Phys. **A505**, 267 (1989).
[33] A. Ramos, A. Polls and W.H. Dickhoff, Nucl. Phys. **A503**, 1 (1989).
[34] W.J.W. Geurts, K. Allaart, W.H. Dickhoff and H. Müther, Phys. Rev. C **53**, 2207 (1996).
[35] A. Polls, M. Radici, S. Boffi, W. H. Dickhoff and H. Müther, Phys. Rev. C **55**, 810 (1997).
[36] *Modern Topics in Electron Scattering*, Eds. B. Frois and I. Sick (World Scientific, Singapore, 1991).
[37] S. Turck-Chièze, Lecture Notes in Physics, **137**, 251 (1981).
[38] O. Benhar, V.R. Pandharipande and S.C. Pieper, Rev. Mod. Phys. **65**, 817 (1993).
[39] D. Rohe *et al*, Phys. Rev. Lett. **93**, 182501 (2004).
[40] S.C. Pieper, private communication.
[41] S.C. Pieper, R.B. Wiringa and V.R. Pandharipande, Phys. Rev. C **46**, 1741 (1992).
[42] G. Garino *et al*, Phys. Rev. C **45**, 78 (1992).
[43] T.G. O'Neill *et al*, Phys. Lett. **B351**, 87 (1995).
[44] D. Abbott *et al*, Phys. Rev. Lett. **80**, 5072 (1998).
[45] K. Garrow *et al*, Phys. Rev. C **66**, 044613 (2002).
[46] Y. Horikawa, F. Lenz and N.C. Mukhopadhyay, Phys. Rev. C **22**, 1680 (1980).
[47] R.J. Glauber, *Lectures in Theoretical Physics*, Eds. W.E. Brittin *et al.* (Interscience, New York, 1959).
[48] D. Rohe *et al.*, nucl-ex/0506007. Submitted for publication in Phys. Rev. C.
[49] G. Höhler *et al.*, Nucl. Phys. **B114**, 505 (1976).
[50] E.J. Brash, A. Kozlov, Sh. Li, and G.M. Huber, Phys. Rev. C **65**, 051001(R) (2002).
[51] M.K. Jones *et al.*, Phys. Rev. Lett. **84**, 1398 (2000).
[52] A. Bodek and J.L. Ritchie, Phys. Rev. D **23**, 1070 (1981).
[53] T.G. O'Neill, private communication.
[54] V.R. Pandharipande and S.C. Pieper, Phys. Rev. C **45**, 791 (1992).
[55] M. Anghinolfi *et al.*, Nucl. Phys. **A602**, 405 (1996).
[56] http://hallcweb.jlab.org/resdata/, and C.E. Keppel, Ph.D. thesis (The American University, 1995)
[57] http://www.jlab.org∼christy/cs_fits/cs_fits.html
[58] J. Arrington *et al*, Phys. Rev. Lett. **82**, 2056 (1999).
[59] J.D. Walecka, *Theoretical Nuclear and Subnuclear Physics* (Oxford University Press, 1995).
[60] C.E. Keppel, private communication.
[61] A. Fabrocini, Phys. Rev. C **55**, 338 (1997).
[62] J. Nieves, J.E. Amaro, M. Valverde and E. Oset, nucl-th/0503023. To appear in the Proceedings of the RCCN Workshop on "Sub-Dominant Oscillation Effects in Atmospheric Neutrino Experiment"